

On new alkaline sulfatometallates: Cs₆[(WO₂)₂O(SO₄)₄], K₈[(MoO₂)₂(SO₄)₆], K_{7.9}Sr_{0.1}[(WO₂)₂(SO₄)₆] and Na₄[MoO₂(SO₄)₃]

Vivien Wessels, Matthias Hämmer, Narayan Simrit Kaur, Lkhamsuren Bayarjargal, Henning A. Höpfe

Angaben zur Veröffentlichung / Publication details:

Wessels, Vivien, Matthias Hämmer, Narayan Simrit Kaur, Lkhamsuren Bayarjargal, and Henning A. Höpfe. 2026. "On new alkaline sulfatometallates: Cs₆[(WO₂)₂O(SO₄)₄], K₈[(MoO₂)₂(SO₄)₆], K_{7.9}Sr_{0.1}[(WO₂)₂(SO₄)₆] and Na₄[MoO₂(SO₄)₃]." *Zeitschrift für anorganische und allgemeine Chemie* 652 (4): e202500168.
<https://doi.org/10.1002/zaac.202500168>.

RESEARCH ARTICLE OPEN ACCESS

On New Alkaline Sulfatometallates: $\text{Cs}_6[(\text{WO}_2)_2\text{O}(\text{SO}_4)_4]$, $\text{K}_8[(\text{MoO}_2)_2(\text{SO}_4)_6]$, $\text{K}_{7.9}\text{Sr}_{0.1}[(\text{WO}_2)_2(\text{SO}_4)_6]$ and $\text{Na}_4[\text{MoO}_2(\text{SO}_4)_3]$

 Vivien Wessels¹  | Matthias Hämmer¹  | Narayan Simrit Kaur¹ | Lkhamsuren Bayarjargal²  | Henning A. Höppe¹ 
¹Professur für Festkörperchemie und Materialwissenschaften, Institute of Physics, Universität Augsburg, Augsburg, Germany | ²Institut für Geowissenschaften, Universität Frankfurt, Frankfurt, Germany

Correspondence: Henning A. Höppe (henning.hoeppe@uni-a.de)

Received: 12 August 2025 | **Revised:** 19 November 2025 | **Accepted:** 20 November 2025

Keywords: caesium | potassium | silicate-analogous | sodium | sulfatomolybdate | sulfatotungstate

ABSTRACT

The new sulfatotungstate $\text{Cs}_6[(\text{WO}_2)_2\text{O}(\text{SO}_4)_4]$ exhibits a hitherto unknown anion with an unusual W–O–W angle of 180° and edge-sharing WO_6 and SO_4 polyhedra. It crystallises in the monoclinic space group $P2_1/c$ (no. 14) with $Z = 2$, determined by single-crystal X-ray diffraction. $\text{K}_8[(\text{MoO}_2)_2(\text{SO}_4)_6]$ and $\text{K}_{7.9}\text{Sr}_{0.1}[(\text{WO}_2)_2(\text{SO}_4)_6]$ crystallise isotypic to each other in the monoclinic space group $P2_1/n$ (no. 14) with $Z = 2$. $\text{Na}_4[\text{MoO}_2(\text{SO}_4)_3]$ crystallises in the orthorhombic non-centrosymmetric space group $P2_12_12_1$ (no. 19) with $Z = 4$, confirmed by second harmonic generation measurements. UV–vis measurements show a bright absorption below 400 nm for all compounds due to the ligand-to-metal charge transfer (LMCT) in tungstate and molybdate moieties. In the fluorescence spectra $\text{Cs}_6[(\text{WO}_2)_2\text{O}(\text{SO}_4)_4]$, $\text{K}_8[(\text{MoO}_2)_2(\text{SO}_4)_6]$ and $\text{K}_{7.9}\text{Sr}_{0.1}[(\text{WO}_2)_2(\text{SO}_4)_6]$ show an emission of the LMCT. Further, all compounds were characterised by FT-IR spectroscopy and thermogravimetric analysis. Latter reveals remarkably high thermal stabilities, especially for $\text{Cs}_6[(\text{WO}_2)_2\text{O}(\text{SO}_4)_4]$.

1 | Introduction

Sulfatotungstates and sulfatomolybdates can be classified as silicate-analogous materials due to the SO_4 tetrahedral building units, such as in borosulfates [1–4], fluorooxoborates [5–7] and polyphosphates [8, 9]. By introducing different moieties, such as sulfates, molybdates or tungstates, the ionic charge of polyhedral centres might change with respect to pure silicates, but above all, enable further opportunities for different coordination geometries and material properties. Due to their optical properties, tungstates and molybdates are classical luminescent materials which are capable of forming MO_4 tetrahedra, MO_5 moieties and MO_6 octahedra with $M = \text{W}, \text{Mo}$ [10–16]. They have been widely used for several decades as laser materials, scintillators or as phosphors in lamp devices [17–19]. They are also

employed as host structures to be doped with rare-earth elements [19]. They act as sensitizers due to their highly efficient charge transfer transitions whose energy can be transferred onto adjacent rare-earth ions, also known as the antenna effect, as, for example, in $\text{Na}_2\text{Y}(\text{PO}_4)(\text{WO}_4) \cdot \text{R}$ ($\text{R} = \text{Eu}, \text{Tb}$) [20], $\text{Gd}_3\text{Cl}_3[\text{WO}_6] \cdot \text{R}$ ($\text{R} = \text{Eu}, \text{Tb}$) [21] or $\text{La}_3\text{Cl}_3[\text{MoO}_6] \cdot \text{Eu}$ [22].

Based on the dissolution of transition metal oxides in molten alkali pyrosulfates—used as a catalysts in the sulfuric acid production to oxidise SO_2 to SO_3 —different studies precipitated novel sulfate compounds from melts containing potassium pyrosulfate. It confirms that $\text{K}_2\text{S}_2\text{O}_7$ is able to dissolve the oxides V_2O_5 , Nb_2O_5 , Ta_2O_5 , MoO_3 and WO_3 [23–26]. In 1998, Noerbygaard et al. were able to synthesise a sulfatomolybdate, the first phase of $\text{K}_2[\text{MoO}_2(\text{SO}_4)_2]$ out of such a melt [27], the future γ -phase [28]. Recently, we discovered a second phase,

Dedicated to the memory of Prof. Dr. Harald Hillebrecht.

 This is an open access article under the terms of the [Creative Commons Attribution](https://creativecommons.org/licenses/by/4.0/) License, which permits use, distribution and reproduction in any medium, provided the original work is properly cited.

 © 2026 The Author(s). *Zeitschrift für anorganische und allgemeine Chemie* published by Wiley-VCH GmbH.

viz., α -K₂[MoO₂(SO₄)₂] [29]. In 2005, Schäffer et al. discovered the first sulfatotungstate K₈[(WO₂)₂(SO₄)₆] with discrete [(WO₂)₂(SO₄)₆]⁸⁻ dimeric units [30]. The same authors discovered the first sodium sulfatomolybdate Na₄[MoO₂(SO₄)₃] a few years later [31]. However, despite some Raman studies, no further characterisation of these compounds was performed yet.

Since both, sulfates and tungstates or molybdates, are excellent host materials for rare-earth ions, sulfatotungstates and sulfatomolybdates seem to be a promising rather new material class. We started to investigate new compounds and are pleased to present the first caesium sulfatotungstate, namely Cs₆[(WO₂)₂O(SO₄)₄]. Furthermore, we will give a deeper insight into the optical and thermal properties of Na₄[MoO₂(SO₄)₃] and K_{7,9}Sr_{0,1}[(WO₂)₂(SO₄)₆]. We will also present the new sulfatomolybdate K₈[(MoO₂)₂(SO₄)₆], which is isotopic to the latter. We elucidated the crystal structures of all titled compounds and characterised them by FT-IR, UV-vis and luminescence spectroscopy and thermogravimetric analysis (TGA).

2 | Results and Discussion

2.1 | Crystal Structures

2.1.1 | Cs₆[(WO₂)₂O(SO₄)₄]

Cs₆[(WO₂)₂O(SO₄)₄] crystallises in a new structure type in the monoclinic space group *P*2₁/*c* (no. 14) with two formula units per unit cell (Figure 1). The anion of the fundamental building unit (FBU) [(WO₂)₂O(SO₄)₄]⁶⁻ is reported for the first time. It is formed by two tungstate octahedra sharing one common corner and are further connected to two sulfate tetrahedra each via common corners (S2) and edges (S1), respectively. To the best of our knowledge, the only edge sharing of SO₄ tetrahedra and tungstate polyhedra in the solid state was reported for WO(SO₄)₂ with a pentagonal bipyramidal coordination of the tungsten atom [32]. The FBU in Cs₆[(WO₂)₂O(SO₄)₄] is not further condensed and is thus classified as 0D according to Liebau. Within, two tungstate octahedra are connected via the bridging oxygen atom

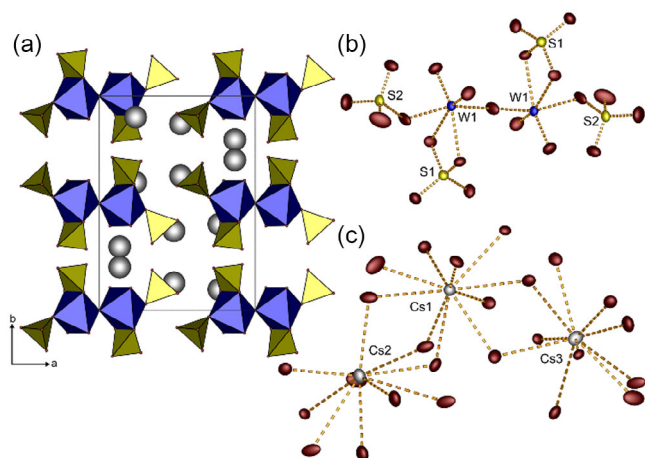


FIGURE 1 | (a) Unit cell of Cs₆[(WO₂)₂O(SO₄)₄] along the *c*-axis, (b) fundamental building unit of the anionic host structure showing a W–O–W angle of 180° and (c) coordination environment of the caesium cations. Sulfate tetrahedra, yellow; tungstate octahedra, blue; caesium cations, grey. Ellipsoids are set to a probability of 50%.

O14 which features an unusual W–O–W angle of 180°. Single-crystal diffraction measurements at low temperature confirmed this angle, and the anisotropic displacement parameters do not show unusual features (Figure S10, Tables S1, S4–5, S12), although some vibration perpendicular to the W–O–W axis is observed at room temperature—so there is indeed some movement. All atoms are assigned to the general Wyckoff position 4*e*, except for the bridging oxygen atom O3 in W–O–W which is assigned to the special position 2*c*, situated on an inversion centre.

The charge balancing caesium cations Cs1, Cs2 and Cs3 are coordinated by 10 oxygen atoms which was confirmed by Madelung Part of Lattice Energy (MAPLE) calculations [33–36].

The W–O bond lengths vary between 172 and 221 pm while S–O bond lengths vary only between 143 and 154 pm. The distances towards bridging oxygen atoms within the FBU are significantly longer due to repulsion of S⁶⁺ and W⁶⁺ centres. Particularly the bond lengths towards the edge sharing tungstate and sulfate polyhedra are elongated. Compared towards only corner sharing polyhedra, they show a significant W–O bond elongation with 221 pm. Contrarily, the tungstate unit exhibits the shortest bond lengths towards the terminal oxygen atoms O4 and O12 with only 172 pm. Also, the S–O bond lengths in the edge sharing sulfate tetrahedron show clear elongations towards the tungstate unit due to repulsion; terminal S–O bond lengths are 144 pm, bridging ones 151 pm. Nevertheless, the average bond lengths of 196 pm (W–O) and 147 pm (S–O) agree well with the sum of the ionic radii according to Shannon (W–O: 198 pm, S–O: 150 pm) [37]. Selected interatomic distances and angles are given in Table 1, a list of selected ionic radii after Shannon is given in Table S14. The different lengths towards oxygen atoms are reflected in the polyhedron deviations calculated by the method of Balić-Zunić and Makovicky [38, 39]. The tungstate octahedron shows a relatively high deviation of –2.98%, the sulfate tetrahedra show smaller deviations with only –0.39% (S1) and –0.08% (S2). SiO₄²⁻ exhibits a slightly larger polyhedron deviation than S₂O₄²⁻ due to sharing an edge with the tungstate octahedron, also revealing a relatively small O–S–O angle of only 99.8°. Nevertheless, the sulfate tetrahedra can be classified as regular tetrahedra. The average Cs–O coordination distances are 319 pm (Cs1) and 332 pm (Cs2, Cs3), which is slightly above the expected distance 319 pm according to Shannon's ionic radii considering a tenfold coordination of caesium [37].

TABLE 1 | Selected interatomic distances/pm and angles/° in Cs₆[(WO₂)₂O(SO₄)₄]. Standard deviations are given in parentheses.

Cs–O	302.18(44)–398.88(46)
$\Sigma r_{ion}(Cs-O)$	316
W–O ^{term.}	172.12(45)–172.58(45)
W–O ^{br.}	187.95(2)–221.38(43)
S–O ^{term.}	143.80(47)–144.79(47)
S–O ^{br.}	151.52(44)–153.76(47)
O–W–O	63.30(14)–160.85(13)
O–S–O	99.8(2)–112.8(3)
W–O–W	179.999(14)

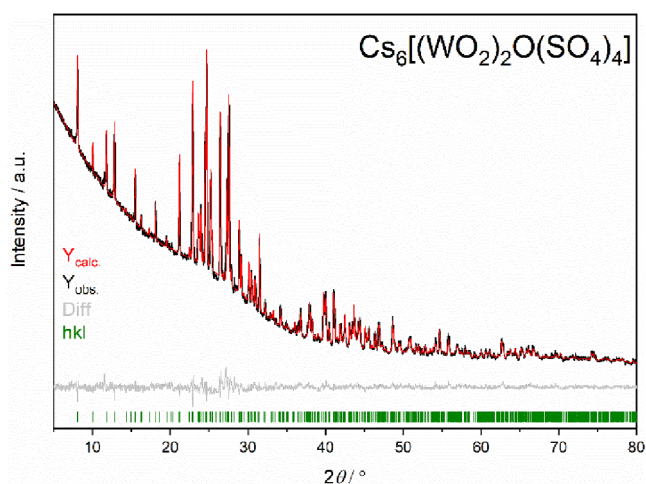


FIGURE 2 | Experimental X-ray diffraction pattern and Rietveld refinement of $\text{Cs}_6[(\text{WO}_2)_2\text{O}(\text{SO}_4)_4]$.

A phase-pure crystalline powder was obtained. The corresponding X-ray diffraction pattern and Rietveld refinement is shown in Figure 2.

2.1.2 | $\text{K}_8[(\text{MoO}_2)_2(\text{SO}_4)_6]$, $\text{K}_{7.9}\text{Sr}_{0.1}[(\text{WO}_2)_2(\text{SO}_4)_6]$

Both compounds crystallise isotypically in the monoclinic space group $P2_1/n$ (no. 14) with two formula units per unit cell. $\text{K}_8[(\text{MoO}_2)_2(\text{SO}_4)_6]$ is reported for the first time and is discussed as representative (Figure 3). All atoms are assigned to the general Wyckoff position 4e. The FBU $[(\text{MoO}_2)_2(\text{SO}_4)_6]^{8-}$ comprises a dimeric unit with two molybdate octahedra connected via two bridging sulfate tetrahedra (S1) forming a vierer ring. This vierer ring is further connected via four sulfate tetrahedra sharing common corners with the molybdate octahedra. The unit is not further condensed and thus classified as 0D according to Liebau. The charge balancing potassium cations are coordinated by nine

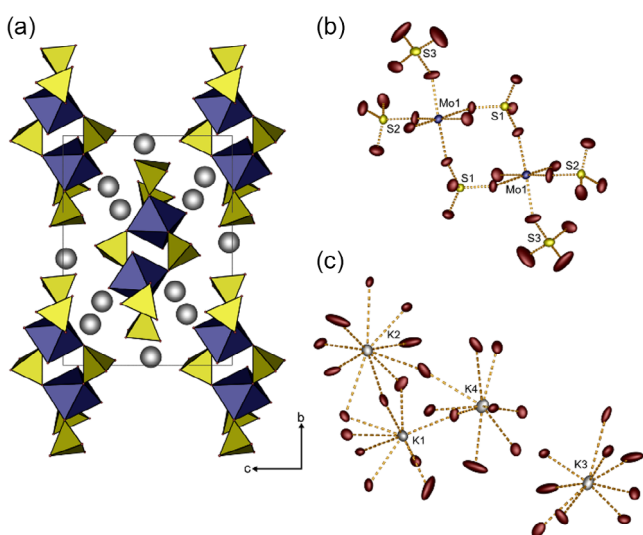


FIGURE 3 | (a) Unit cell of $\text{K}_8[(\text{MoO}_2)_2(\text{SO}_4)_6]$ along the a -axis, (b) fundamental building unit of the anionic host structure showing a vierer ring and (c) coordination environment of the potassium cations. Sulfate tetrahedra, yellow; molybdate octahedra, violet; potassium cations, grey. Ellipsoids are set to a probability of 50%.

(K1, K3, K4) and ten (K2) oxygen atoms, respectively, which was proven by MAPLE calculations [33–36].

The average Mo–O bond length is 196 pm which is close to the expected interatomic distance according to Shannon's radii with 197 pm [37]. The average S–O bond length is 147 pm which is close to the expected distance after Shannon with 150 pm [37]. This is also reflected in small polyhedral deviations for the sulfate tetrahedra (S1: -0.11% , S2: -0.07% , S3: -0.12%). Contrarily, the deviation of the molybdate octahedron is with a value of -7.18% remarkably large. The Mo^{6+} in the centre is bent strongly towards the terminal oxygen ligands O1 and O2 with significantly shorter bond lengths of 168 and 169 pm due to repulsion of four neighboured S^{6+} centres and the tension of the vierer ring which explains the large polyhedron deviation. The average bond length between the potassium cations and corresponding oxygen ligands amounts to 296 pm for K1, K3 and K4 with a coordination number (CN) of 9 and 302 pm for K2 with a CN of 10. Both values are slightly higher than the expected ionic radii according to Shannon with 293 pm in case of CN = 9 and 297 pm for CN = 10 [37].

2.1.3 | $\text{Na}_4[\text{MoO}_2(\text{SO}_4)_3]$

The sodium sulfatomolybdate $\text{Na}_4[\text{MoO}_2(\text{SO}_4)_3]$ crystallises in the non-centrosymmetric orthorhombic space group $P2_12_12_1$ (no. 19) with four formula units per unit cell (Figure 4). The absence of an inversion centre was proven by second harmonic generation (SHG) measurements (Table S11). All atoms are assigned to the general Wyckoff position 4a. The FBU consists of one molybdate octahedron connected towards three sulfate tetrahedra via common edges. These units are further condensed forming a zig-zag chain along the a -axis. Thus, the anionic host structure can be classified as 1D according to Liebau. The sodium cations are coordinated by six oxygen atoms each, proven by MAPLE calculations [33–36].

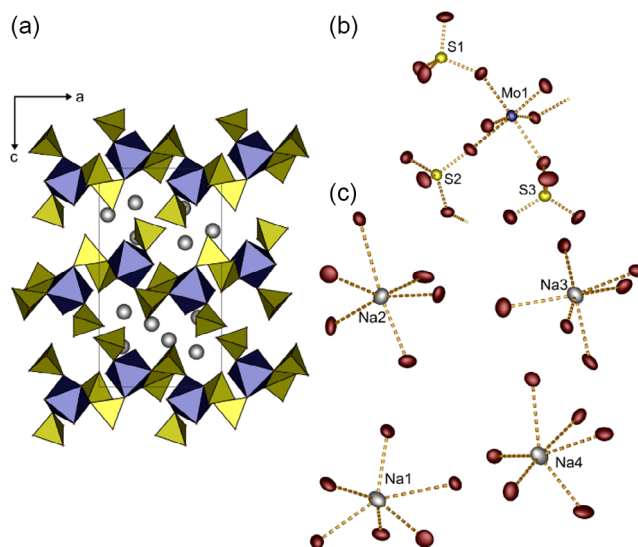


FIGURE 4 | (a) Unit cell of $\text{Na}_4[\text{MoO}_2(\text{SO}_4)_3]$ along the a -axis, (b) fundamental building unit of the anionic host structure which is further connected to 1D chain and (c) coordination environment of the sodium cations. Sulfate tetrahedra, yellow; molybdate octahedra, violet; sodium cations, grey. Ellipsoids are set to a probability of 50%.

The average Mo–O and S–O bond lengths are 195 and 147 pm, respectively, which is in accordance with Shannon's ionic radii (Mo–O: 197 pm and S–O: 150 pm). Polyhedron deviations of the sulfate tetrahedra are insignificant with values of –0.04% (S1), –0.07% (S2) and –0.09% (S3) and can be classified as regular polyhedra [38, 39]. The molybdate octahedron shows with –5.71% a large deviation due to the repulsion of neighbouring sulfate tetrahedra. This is reflected in shorter bond lengths towards the two terminal oxygen atoms (O2: 168 pm, O1: 170 pm). The average interatomic distance between sodium cations and oxygen ligands is 247 pm and thus slightly larger than the expected value of 240 pm after Shannon considering a sixfold coordination of sodium [37].

2.2 | Electrostatic Calculations

All crystal structures were examined for their electrostatic consistency with calculations based on the MAPLE concept [33–36]. The single-crystal data of the compounds were used to calculate their MAPLE values and were compared to the MAPLE values of the binary and tertiary compounds (Tables 2 and S12). Deviations remain below 1% which indicates electrostatic consistency of the structure model. We considered a full occupation of the cation sites in $K_{7.9}Sr_{0.1}[(WO_2)_2(SO_4)_6]$.

2.3 | UV-Vis and Vibrational Spectroscopy

Optical properties of all compounds were investigated by recording UV-vis spectra. All compounds show a high reflection in the visible region and broad absorption bands below 400 nm due to the ligand-to-metal charge transfer (LMCT) within either the molybdate or tungstate units (Figure 5a). These transitions are parity allowed and therefore very pronounced. $Na_4[MoO_2(SO_4)_3]$ reveals an additional band around 450 nm. We recently discovered a minimal presence of Mo^{5+} in α - $K_2[MoO_2(SO_4)_2]$ by electron spin resonance (ESR) measurements which enables d–d transitions in sulfatomolybdates [29]. Such transitions are the reason for different hues of the powder samples. Since molybdenum and tungsten possess very similar chemical properties due to their position in the periodic table, we can assume small amounts of W^{5+} in the tungstate compounds as well. While $K_{7.9}Sr_{0.1}[(WO_2)_2(SO_4)_6]$ appears colourless, $K_8[(MoO_2)_2(SO_4)_6]$ exhibits a light blue hue which is reflected in the UV-vis spectrum, as the highest reflection occurs in the bluish region. This is similar for $Cs_6[(WO_2)_2O(SO_4)_4]$, where the highest reflection point is slightly shifted to longer wavelengths, yielding a turquoise hue. $Na_4[MoO_2(SO_4)_3]$ appears light green due to an additional absorption band in the blue region. The colourless impression of $K_{7.9}Sr_{0.1}[(WO_2)_2(SO_4)_6]$ indicates, that the defects on the potassium sites caused by the presence of M^{5+} in the anion, are healed by the strontium doping.

TABLE 2 | Calculated MAPLE values of $Cs_6[(WO_2)_2O(SO_4)_4]$, $K_8[(WO_2)_2(SO_4)_6]$, $K_8[(MoO_2)_2(SO_4)_6]$ and $Na_4[MoO_2(SO_4)_3]$ compared to the binary and tertiary compounds.

$Cs_6[(WO_2)_2O(SO_4)_4]$ (SC-XRD) MAPLE = 179 610 kJ mol ⁻¹ Δ = 0.14%	3 Cs ₂ SO ₄ [40] + 2 WO ₃ [41] + SO ₃ [42] MAPLE = 179 864 kJ mol ⁻¹
$K_8[(WO_2)_2(SO_4)_6]$ (SC-XRD) MAPLE = 245 914 kJ mol ⁻¹ Δ = 0.72%	4 K ₂ SO ₄ [43] + 2 WO ₃ [41] + 2 SO ₃ [42] MAPLE = 244 144 kJ mol ⁻¹
$K_8[(MoO_2)_2(SO_4)_6]$ (SC-XRD) MAPLE = 245 172 kJ mol ⁻¹ Δ = 0.56%	4 K ₂ SO ₄ [43] + 2 MoO ₃ [44] + 2 SO ₃ [42] MAPLE = 243 791
$Na_4[MoO_2(SO_4)_3]$ (SC-XRD) MAPLE = 122 477 kJ mol ⁻¹ Δ = 0.90%	2 Na ₂ O [45] + MoO ₃ [44] + 3 SO ₃ [42] MAPLE = 121 374 kJ mol ⁻¹

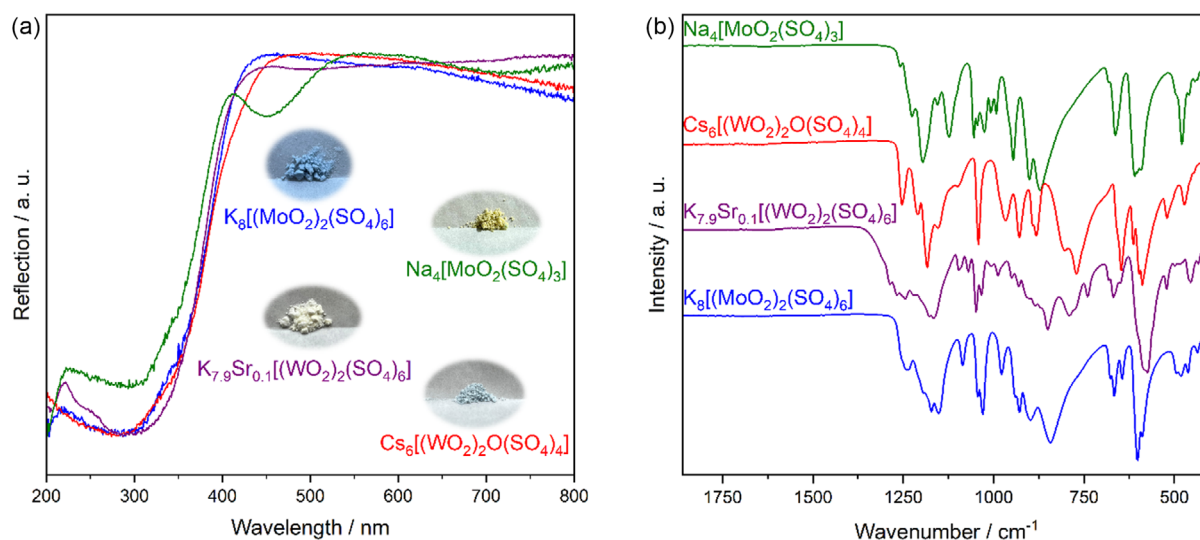


FIGURE 5 | (a) UV-vis spectra of the investigated sulfatungstates and sulfatomolybdates and (b) their FT-IR spectra.

The absorption edges of the titled compounds are in accordance with known tungstates and molybdates exhibiting $[\text{WO}_6]^{6-}$ and $[\text{MoO}_6]^{6-}$ moieties, such as in $\text{Ni}(\text{MoO}_4)$ and $\text{R}_2(\text{WO}_6)$ [16, 46], and will be roughly discussed in the following chapter.

The FT-IR spectra show typical vibrations in the region between 1400 and 400 cm^{-1} for all compounds (Figures 5b and S4). The absence of O–H bonds is confirmed by the absence of any bands between 4000 and 1400 cm^{-1} . Even after months of storing the compounds under ambient atmosphere, no O–H vibrations show up in the FT-IR spectra. Thus, all titled compounds seem to be stable at air. The assignment of vibrational bands is based on the previously discussed sulfatotungstates and sulfatomolybdates [47]. Bands between 1400 and 950 cm^{-1} can be assigned to symmetric $\nu_{\text{sym.}}(\text{S-O})$ and asymmetric $\nu_{\text{asym.}}(\text{S-O})$ vibrations in the sulfate moieties. Appropriate bending vibrations $\delta(\text{S-O})$ occur between 650 and 400 cm^{-1} [48–52]. W–O–W vibrations $\nu(\text{W-O-W})$ in corner sharing tungstate octahedra are found between 870 and 610 cm^{-1} . Thus, out of all compounds discussed, $\text{Cs}_6[(\text{WO}_2)_2\text{O}(\text{SO}_4)_4]$ shows the most pronounced band in this region due to its W–O–W bridge inside the FBU (Figure 1). Further vibrations between the transition metals and oxygen are assigned as follows; 960–600 cm^{-1} towards $\nu_{\text{sym.}}(\text{W-O})$ and $\nu_{\text{asym.}}(\text{W-O})$, 990–600 cm^{-1} towards $\nu_{\text{sym.}}(\text{Mo-O})$ and $\nu_{\text{asym.}}(\text{Mo-O})$. Bending vibrations $\delta(\text{W-O})$ and $\delta(\text{Mo-O})$ are found below 500 and 400 cm^{-1} , respectively, the latter is already out of the recorded region [53–57].

2.4 | Fluorescence Spectroscopy

To investigate the emission of the LMCT of the tungstate and molybdate units, photoluminescence spectra were recorded. The photoluminescence spectra of so far investigated sulfatotungstates $\text{M}_2[\text{W}_2\text{O}_3(\text{SO}_4)_6]$ ($\text{M} = \text{Y}, \text{Sm}, \text{Eu}, \text{Gd}, \text{Tb}, \text{Ho}, \text{Lu}, \text{Bi}$) did not reveal any emission due to a LMCT [47]. Contrarily, $\text{K}_{7,9}\text{Sr}_{0,1}[(\text{WO}_2)_2(\text{SO}_4)_6]$ and $\text{Cs}_6[(\text{WO}_2)_2\text{O}(\text{SO}_4)_4]$ indeed show broad excitation and emission bands (Figure 6a, c). Excitation occurs in the UV, while the emission takes place in the green region of the visible spectrum peaking at 509 nm for $\text{K}_{7,9}\text{Sr}_{0,1}[(\text{WO}_2)_2(\text{SO}_4)_6]$ and 516 nm for $\text{Cs}_6[(\text{WO}_2)_2\text{O}(\text{SO}_4)_4]$. This is expected for tungstates with sixfold coordination, such as in $\text{R}_2(\text{WO}_6)$ and $\text{Ln}_3\text{Cl}_3[\text{WO}_6]$ [21, 46, 58]. The sulfatomolybdates seem to show weaker luminescence intensities, as $\text{K}_8[(\text{MoO}_2)_2(\text{SO}_4)_6]$ (Figure 6b) exhibits lower intensities than $\text{K}_{7,9}\text{Sr}_{0,1}[(\text{WO}_2)_2(\text{SO}_4)_6]$. We suggest that this might be caused

by the strontium doping, thus avoiding defects on the potassium sites caused by the presence of W^{5+} in the sulfatotungstate. The noisy structure around in the broad-banded emission of $\text{K}_8[(\text{MoO}_2)_2(\text{SO}_4)_6]$ peaking at 467 nm is assigned to artefacts of the xenon discharge lamp of the measurement device as often seen for weak emission intensities. The spin–orbit coupling is much stronger for tungsten than for molybdenum; accordingly, the emission from the lowest lying triplet LMCT states is fostered in the tungstates. $\text{Na}_4[\text{MoO}_2(\text{SO}_4)_3]$ did not show any detectable luminescence at room temperature at all; as far as we can suggest, there seems to be no correlation with the FBU and the dimensionality of the anion since $\alpha\text{-K}_2[\text{MoO}_2(\text{SO}_4)_2]$ does show luminescence—exhibiting a 3D host structure [29]. A feasible reason for the absence of emission in $\text{Na}_4[\text{MoO}_2(\text{SO}_4)_3]$ might be the absorption band in the blue region (Figure 5). Also compounds such as M_2MoO_6 ($\text{M} = \text{La}, \text{Y}, \text{Gd}, \text{Lu}$) do not show any emission as reported by Blasse, whereas the respective tungstate compounds exhibit emission in the blue (Table S13) [58].

Comparing the isotopic structures $\text{K}_8[(\text{MoO}_2)_2(\text{SO}_4)_6]$ and $\text{K}_{7,9}\text{Sr}_{0,1}[(\text{WO}_2)_2(\text{SO}_4)_6]$, the bandgaps determined via Tauc plots (Figure S5) based on the UV–vis spectra of both compounds reveal a slight shift towards higher values from molybdate to tungstates, as expected.

Contrarily, the excitation and emission maxima of both, displayed in Figure 6a,b, shift to higher energies from the tungstate towards the molybdate. This trend might be surprising since Mo(VI) is less stable against reduction than W(VI), but the significantly stronger spin–orbit coupling in tungsten stabilises the lowest lying LMCT triplet states better than Mo(VI); accordingly, the respective emission energies can also be lower for tungstates compared with molybdates [59]. A comparison of excitation and emission energies with other tungstate and molybdate compounds are listed in Table S13.

2.5 | Thermal Analysis

The thermal stability was investigated by TGA measurements. Relative stabilities are summarised in Table 3, respective diagrams are presented in Figures S6–9. All decompositions occur in a single large step, presumably by releasing SO_3 . The compounds show remarkably high thermal stabilities, especially those with lower dimensionalities of the anion. $\text{Cs}_6[(\text{WO}_2)_2\text{O}(\text{SO}_4)_4]$ shows with 700°C the highest stability so far for these material classes. Compared to the thermal stabilities

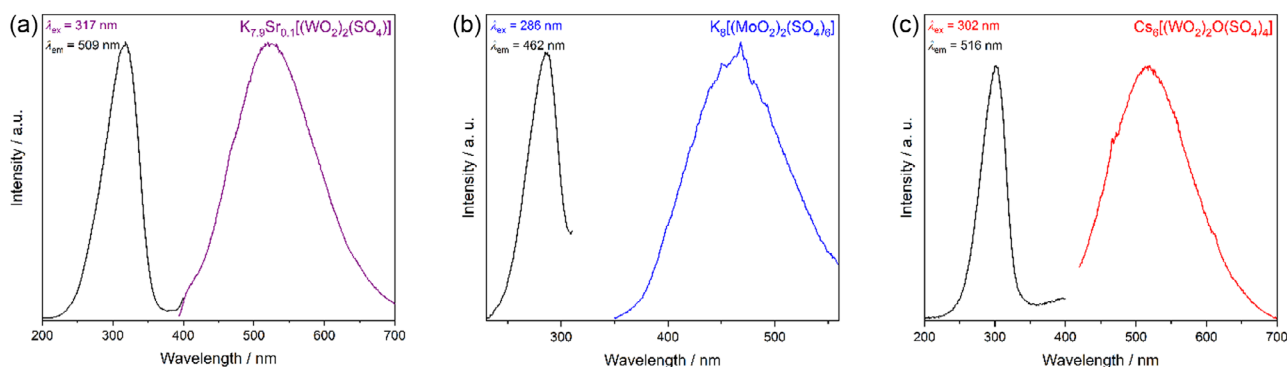


FIGURE 6 | Respective emission and excitation spectra of (a) $\text{K}_{7,9}\text{Sr}_{0,1}[(\text{WO}_2)_2(\text{SO}_4)_6]$, (b) $\text{K}_8[(\text{MoO}_2)_2(\text{SO}_4)_6]$ and (c) $\text{Cs}_6[(\text{WO}_2)_2\text{O}(\text{SO}_4)_4]$.

TABLE 3 | Thermal stabilities of investigated sulfatomolybdates and sulfatotungstates.

Compound	Decomposition Temperature/°C
Cs ₆ [(WO ₂) ₂ O(SO ₄) ₄]	700
K ₈ [(MoO ₂) ₂ (SO ₄) ₆]	560
K _{7.9} Sr _{0.1} [(WO ₂) ₂ (SO ₄) ₆]	540
Na ₄ [MoO ₂ (SO ₄) ₃]	436

in M₂[W₂O₃(SO₄)₆] (M = Y, Sm, Eu, Gd, Tb, Ho, Lu, Bi)—also containing 0D anions—the stabilities of the sulfatotungstates in this work are slightly higher (e.g., Bi₂[W₂O₃(SO₄)₆]: 320°C, Lu₂[W₂O₃(SO₄)₆]: 510°C) [47], probably due to lower charged cations reducing the repulsion forces in the lattice. Materials with lower dimensionalities might be more stable due to less repulsion between the highly charged centres S⁶⁺, Mo⁶⁺ and W⁶⁺. This trend was also observed in borosulfates and previous work on phases of K₂[MoO₂(SO₄)₂] with differing dimensionalities [4, 60–62]. The ionic radius of the cation might also play an important role regarding the thermal stabilities of the materials, as they influence the lattice energy. In the isotypic series M₂[W₂O₃(SO₄)₆] (M = Y, Sm, Eu, Gd, Tb, Ho, Lu, Bi) we observed a decrease of the thermal stability with increasing ionic radius of the cation M³⁺.

3 | Conclusions

Herein, we elucidated sulfatotungstates and sulfatomolybdates by introducing three new compounds. Cs₆[(WO₂)₂O(SO₄)₄] features an unprecedented anion showing an unusual W–O–W angle of 180°. It comprises the first sulfatotungstate which consists of edge-sharing WO₆ and SO₄ polyhedra. Further, it marks the first caesium compound in this material class. Next to this, the compounds K₈[(MoO₂)₂(SO₄)₆], K_{7.9}Sr_{0.1}[(WO₂)₂(SO₄)₆] and Na₄[MoO₂(SO₄)₃] were considered. We discussed the crystal structures in detail, confirmed them by MAPLE calculations and expanded the knowledge of such compounds by discussing their optical and thermal properties.

UV–vis spectroscopy revealed broad absorption bands below 400 nm due to the LMCT of the molybdate and tungstate octahedral units in the crystal structure. Fluorescence spectroscopy confirmed this transition for Cs₆[(WO₂)₂O(SO₄)₄], K₈[(MoO₂)₂(SO₄)₆], K_{7.9}Sr_{0.1}[(WO₂)₂(SO₄)₆] and Na₄[MoO₂(SO₄)₃] did not show any detectable luminescence at room temperature. The titled compounds showed remarkably high thermal stabilities with decomposition temperature above 400°C. Cs₆[(WO₂)₂O(SO₄)₄] in particular exhibits a high stability, as decomposition only begins at 700°C.

These findings are promising steps for further investigations of these new material classes as possible antenna phosphors.

4 | Experimental Section

4.1 | Syntheses

All compounds were prepared via melting the educts MO₃ (M = Mo, W), A₂SO₄ and A₂S₂O₇ (A = Na, K, Cs)

stoichiometrically (MoO₃: Fluka, WO₃: Alfa Aesar, Na₂SO₄: Merck, K₂SO₄: VWR, Cs₂SO₄: Chempur, Na₂S₂O₇ was obtained by heating NaHSO₄ (Fluka) at 280°C overnight and was kept in a drying chamber at 180°C afterwards, K₂S₂O₇: Bernd Kraft, stored at 180°C in a drying chamber, Cs₂S₂O₇ was synthesised via CsOH·H₂O (Alfa Aesar) in a nitrogen flushed Schlenk tube in H₂SO₄ by heating the mixture at 200°C for 30 min). The respective educts were ground and filled in a preheated silica ampoule. In case of Cs₆[(WO₂)₂O(SO₄)₄] and K_{7.9}Sr_{0.1}[(WO₂)₂(SO₄)₆] the ampoule was evacuated, K₈[(MoO₂)₂(SO₄)₆] and Na₄[MoO₂(SO₄)₃] could be synthesised either in ambient air or in an evacuated ampoule. Nevertheless, the ampoule was sealed in all cases. Cs₆[(WO₂)₂O(SO₄)₄] was heated to 500°C for 2½ h, hold for 10 h and cooled down in 2½ h to room temperature again. K_{7.9}Sr_{0.1}[(WO₂)₂(SO₄)₆] was heated in 3½ h to 650°C, hold for 10 h and cooled down to 300°C within 70 h and to room temperature again in 1½ h. Both, K₈[(MoO₂)₂(SO₄)₆] and Na₄[MoO₂(SO₄)₃] were synthesised by heating up to 480°C within 2½ h, holding the temperature for 10 h and cooling down to room temperature in 80 h. The crystalline powders were obtained phase-pure (Figures 2 and S1–3). In case of K_{7.9}Sr_{0.1}[(WO₂)₂(SO₄)₆] we could not figure out the origin of the strontium doping. Nevertheless, we proved its presence by energy-dispersive X-ray spectroscopy (Table S17).

4.2 | Crystal Structure Determination

Single-crystal structure determination was enabled by transferring the crystals from the ampoule directly into a perfluorinated polyether for selection. The diffraction data were collected with a Bruker D8 Venture diffractometer using Mo-K_α radiation (λ = 0.71073 Å). Absorption correction was done via the multi-scan method, here direct method was used followed by refinement by the full-matrix least-squares technique with the SHELXTL software package [63, 64]. Crystallographic data for the firstly mentioned compounds Cs₆[(WO₂)₂O(SO₄)₄] and K₈[(MoO₂)₂(SO₄)₆] is summarised in Table 4, further details as well as data for K₈[(WO₂)₂(SO₄)₆] and Na₄[MoO₂(SO₄)₃] is pointed out in Tables S1. For a stable refinement of the strontium doping in K_{7.9}Sr_{0.1}[(WO₂)₂(SO₄)₆] a full occupation of the K/Sr sites was assumed, which also delivered the best residuals; a free refinement is unstable, though, as the electron count of Sr is double the count of K. Maintaining charge balance would require to replace two K atoms by one Sr atom, the electron density on the site would be the same causing the refinement to fail.

4.3 | Rietveld Refinement

Rietveld analysis of Cs₆[(WO₂)₂O(SO₄)₄] was done by means of the programme TOPAS V. 5.0 [65]. The structural model out of single-crystal data was used as starting model. Further data is presented in Table S10.

4.4 | X-Ray Powder Diffraction

The samples were ground and filled in a Hilgenberg silica-glass capillary with a wall thickness of 0.01 mm and an outer diameter 0.3 mm or in case of K₈[(WO₂)₂(SO₄)₆] prepared on a stainless-steel sample holder by flattening the sample with a glass plate.

TABLE 4 | Crystal data and details of the structural refinements of Cs₆[(WO₂)₂O(SO₄)₄] and K₈[(MoO₂)₂(SO₄)₆] determined by single-crystal X-ray diffraction. Standard deviations are given in parentheses.

	Cs ₆ [(WO ₂) ₂ O(SO ₄) ₄]	K ₈ [(MoO ₂) ₂ (SO ₄) ₆]
Temperature/K	297(2)	296(2)
Molar weight/g mol ⁻¹	1629.40	1145.04
Crystal system	Monoclinic	Monoclinic
Space group	<i>P</i> ₂ ₁ / <i>c</i>	<i>P</i> ₂ ₁ / <i>n</i>
<i>a</i> /Å	10.8744(3)	9.4260(3)
<i>b</i> /Å	14.9457(5)	14.0022(4)
<i>c</i> /Å	7.7619(3)	10.3259(4)
β /°	92.7012(10)	90.652(2)
<i>V</i> /Å ³	1260.10(7)	1362.77(8)
<i>Z</i>	2	2
ρ /g mol ⁻¹	4.294	2.794
Absorption coefficient μ /mm ⁻¹	18.076	2.718
F(000)	1420	1112
Radiation; wavelength λ /Å	0.71073	0.71073
Diffractometer	Bruker D8 Venture	Bruker D8 Venture
θ range/°	2.318–27.924	2.451–29.265
Absorption correction	Multi-scan	Multi-scan
Transmission (min; max)	0.589; 0.746	0.6573; 0.7458
Index range	–14/14 –19/19 –10/10	–12/12 –19/19 –14/14
<i>h</i> / <i>k</i> / <i>l</i>		
Reflections collected	30 493	82 407
Independent reflections	3019	3710
Obs. reflections	2490	3125
Refined parameters/restraints	152	200
<i>R</i> _{int}	0.0657	0.1075
<i>R</i> ₁ (all data)	0.0400	0.0455
<i>wR</i> ₂	0.0417	0.0855
GooF	1.045	1.194
Residual electron density (max; min)/e ⁻ Å ⁻³	1.002; –0.954	1.338; –1.507
CSD	2 478 520	2 478 521

Data were collected by either using a Bruker D8 Advance diffractometer using Cu-K α radiation ($\lambda = 1.54184$ Å) with a 1D LynxEye detector system, steps of 0.02° and transmission geometry or by using a Seifert 3003 TT diffractometer with Cu-K α radiation ($\lambda = 1.54184$ Å) and a GEMETEOIR 1D line detector. In both cases, the generator was operated at 40 kV and 40 mA with a scan range between 5° and 80°.

4.5 | Infrared Spectroscopy

Infrared spectra were recorded by means of a Bruker EQUINOX 55 FT-IR spectrometer operating at room temperature with a platinum ATR device and a scan range between 4000 and 400 cm⁻¹, a resolution of 2 cm⁻¹ and running 32 scans per sample.

4.6 | UV-Vis Spectroscopy

UV-vis spectra were recorded as diffuse reflection spectra using a Varian Cary 300 Scan UV-vis spectrophotometer with an Ulbricht sphere detector. It is equipped with a deuterium and mercury lamp as light source; the lamp switch is located at 350 nm. The scan range was between 200 and 800 nm with an increment of 1 nm and a scan rate of 120 nm cm⁻¹.

4.7 | Fluorescence Spectroscopy

The solid-state excitation and emission spectra were recorded with a Horiba FluoreMax-4 fluorescence spectrometer operating at room temperature. A xenon discharge lamp which operates between 200 and 800 nm is equipped as light source.

4.8 | Thermal Analysis

TGA was performed by using alumina crucibles and the device NETZSCH STA 409 PC Luxx in nitrogen atmosphere and a heating ramp of $5^{\circ}\text{C min}^{-1}$.

4.9 | Second Harmonic Generation

SHG measurements were performed on microcrystalline powder samples clamped between two glass slides using the Kurtz–Perry approach [66]. Al_2O_3 , KH_2PO_4 (KDP) and quartz were used as reference materials. A Q-switched Nd:YAG laser (1064 nm, 5–6 ns, 2 kHz) was used for the generation of the fundamental pump wave. The fundamental infrared light was separated using a harmonic separator, a short-pass filter and an interference filter from the generated second harmonic (532 nm). The generated SHG signal was collected with a photomultiplier and an oscilloscope from seven different areas of the sample. On each position, 128 pulses were measured and averaged. Background signals between the laser pulses were used to correct the measured intensities. The SHG measurements were performed under ambient conditions in transmission geometry.

4.10 | Raman Spectroscopy

Raman measurements were carried out with a custom set-up in Frankfurt described in detail elsewhere [67]. We used a laser with the wavelength of $\lambda = 532$ nm (Cobolt-Samba, Hübner Photonics) and a spectrograph (Princeton Instruments ACTON SpectraPro 2300i) equipped with a Pixis256E CCD camera. Measurements were performed in reflection geometry with the polarised laser light.

4.11 | Energy Dispersive X-Ray Spectroscopy

Energy dispersive X-ray spectroscopy was measured with a Zeiss Merlin 450 scanning electron microscope and an Oxford Instruments Ultim Max 170 EDX detector. A summary of the measurement data is depicted in Tables S15–S18.

Acknowledgments

L.B. thanks the Deutsche Forschungsgemeinschaft for generous support under the Project no. 468566236 (BA4020).

Open Access funding enabled and organized by Projekt DEAL.

Funding

This work was supported by the Deutsche Forschungsgemeinschaft (468566236).

Conflicts of Interest

The authors declare no conflicts of interest

Data Availability Statement

The data that support the findings of this study are available from the corresponding author upon reasonable request.

References

1. P. Netzsch, P. Gross, H. Takahashi, and H. A. Höpfe, “Exploring Main Group Metal Borosulfates: Similarities and Differences of Two New Borosulfates $\text{M}[\text{B}_2\text{O}(\text{SO}_4)_3]$ ($\text{M} = \text{Sr}, \text{Pb}$),” *Inorganic Chemistry* 57 (2018): 8530.
2. J. Bruns, H. A. Höpfe, M. Daub, H. Hillebrecht, and H. Huppertz, “Synthesis-Controlled Polymorphism and Optical Properties of Phyllosilicate-Analogous Borosulfates $\text{M}[\text{B}_2(\text{SO}_4)_4]$ ($\text{M} = \text{Mg}, \text{Co}$)” *Chemistry: A European Journal* 26 (2020): 7966.
3. P. Netzsch, P. Gross, H. Takahashi, S. Lotfi, J. Brgoch, and H. A. Höpfe, “On Silicate-Analogous Materials: Synthesis and Characterisation of Novel Borosulfates,” *European Journal of Inorganic Chemistry* 2019 (2019): 3975.
4. P. Netzsch, M. Hämmer, P. Gross, et al., “ $\text{RE}_2[\text{B}_2(\text{SO}_4)_6]$ ($\text{RE} = \text{Y}, \text{La-Nd}, \text{Sm}, \text{Eu}, \text{Tb-Lu}$): A Silicate-Analogous Host Structure with Weak Coordination Behaviour,” *Dalton Transactions* 48 (2019): 4387.
5. S. G. Jantz, F. Pielhofer, L. van Wüllen, R. Wehrich, M. J. Schäfer, and H. A. Höpfe, “The First Alkaline-Earth Fluorooxoborate $\text{Ba}[\text{B}_4\text{O}_6\text{F}_2]$ - Characterisation and Doping with Eu^{2+} ,” *Chemistry – A European Journal* 24 (2018): 443.
6. M. Mutailipu and S. Pan, “Emergent Deep-Ultraviolet Nonlinear Optical Candidates,” *Angewandte Chemie International Edition* 59 (2020): 20302.
7. S. G. Jantz, M. Dialer, L. Bayarjargal, et al., “ $\text{Sn}[\text{B}_2\text{O}_3\text{F}_2]$ —The First Tin Fluorooxoborate as Possible NLO Material,” *Advanced Optical Materials* 6 (2018): 1800497.
8. H. A. Höpfe, K. Kazmierczak, S. Kacprzak, I. Schellenberg, and R. Pöttgen, “Surprising Luminescent Properties of the Polyphosphates $\text{Ln}(\text{PO}_3)_3 : \text{Eu}$ ($\text{Ln} = \text{Y}, \text{Gd}, \text{Lu}$),” *Dalton Transactions* 40 (2011): 9971.
9. H. A. Höpfe and S. J. Sedlmaier, $\text{MH}_2\text{P}_2\text{O}_7$ ($\text{M} = \text{Co}, \text{Ni}$): Metamagnetic Interaction between the Zigzag Octahedral Chains,” *Inorganic Chemistry* 46 (2007): 3467.
10. R. S. Barker and I. Radosavljevic Evans, “Structural Characterization of $\text{RE}(\text{10})\text{W}(\text{22})\text{O}(\text{81})$ Rare-Earth Tungstates ($\text{RE} = \text{Ce}, \text{Nd}$),” *Acta Crystallographica Section B* 64 (2008): 708.
11. P. V. Klevtsov and R. F. Klevtsova, “Polymorphism of the Double Molybdates and Tungstates of Mono- and Trivalent Metals with the Composition $\text{M}^+\text{R}^{3+}(\text{EO}_4)_2$,” *Journal of Structural Chemistry* 18 (1977): 339.
12. J. Chen, X. Yang, C. Jiang, Y. Wang, L. Zhou, and M. Wu, “Effective Enhancement of Mechanical Properties via H/F Substitution in 3D Cyanide Hybrid Perovskites,” *RSC Advances* 12 (2022): 29338.
13. O. Beaury, M. Faucher, and G. Teste de Sagey, “The Structure of Yttrium Tungstate $\epsilon\text{-Y}_2\text{WO}_6$,” *Acta Crystallographica Section B* 37 (1981): 1166.
14. Y.-L. Shen, H.-L. Jiang, J. Xu, J.-G. Mao, and K. W. Cheah, “Luminescent Lanthanide Selenites and Tellurites Decorated by MoO_4 Tetrahedra or MoO_6 Octahedra: $\text{Nd}_2\text{MoSe}_2\text{O}_{10}$, $\text{Gd}_2\text{MoSe}_3\text{O}_{12}$, $\text{La}_2\text{MoTe}_3\text{O}_{12}$, and $\text{Nd}_2\text{MoTe}_3\text{O}_{12}$,” *Inorganic Chemistry* 44 (2005): 9314.
15. M. Hämmer, O. Janka, J. Bönnighausen, S. Klenner, R. Pöttgen, and H. A. Höpfe, “On the Phosphors $\text{Na}_5\text{M}(\text{WO}_4)_4$ ($\text{M} = \text{Y}, \text{La-Nd}, \text{Sm-Lu}, \text{Bi}$) – Crystal Structures, Thermal Decomposition, and Optical and Magnetic Properties,” *Dalton Transactions* 49 (2020): 8209.
16. H. Tian, C. A. Roberts, and I. E. Wachs, “Molecular Structural Determination of Molybdena in Different Environments: Aqueous Solutions, Bulk Mixed Oxides, and Supported MoO_3 Catalysts,” *The Journal of Physical Chemistry C* 114 (2010): 14110.
17. H. A. Höpfe, “Recent Developments in the Field of Inorganic Phosphors,” *Angewandte Chemie International Edition* 48 (2009): 3572.
18. G. Blasse and C. B. Grabmaier, in *Luminescent Materials*, Berlin, Heidelberg: Springer, (1994): 1–9.

19. T. Jüstel, H. Nikol, and C. Ronda, "New Developments in the Field of Luminescent Materials for Lighting and Displays," *Angewandte Chemie International Edition* 37 (1998): 3084.
20. M. Daub, A. J. Lehner, and H. A. Höpfe, "Synthesis, Crystal Structure and Optical Properties of Na 2 RE (PO 4)(WO 4)(RE= Y, Tb–Lu)," *Dalton Transactions* 41 (2012): 12121.
21. K. V. Dorn, B. Blaschkowski, K. Förg, P. Netzsch, H. A. Höpfe, and I. Hartenbach, "Prism Inside: Spectroscopic and Magnetic Properties of the Lanthanide (III) Chloride Oxidotungstates (VI) Ln₃Cl₃ [WO₆](Ln= La–Nd, Sm–Tb)," *Zeitschrift Fur Anorganische Und Allgemeine Chemie* 643 (2017): 1642.
22. K. V. Dorn, B. Blaschkowski, P. Netzsch, H. A. Höpfe, and I. Hartenbach, "Blue Excitement: The Lanthanide (III) Chloride Oxidomolybdates (VI) Ln₃Cl₃ [MoO₆](Ln= La, Pr, and Nd) and their Spectroscopic Properties," *Inorganic Chemistry* 58 (2019): 8308.
23. B. Flemming, R. W. Berg, and K. Nielsen, "The Crystal Structure of K „Nb (SO), and K, Ta (SO)," *Acta Chemica Scandinavica* 44 (1990): 328.
24. N. H. Hansen, R. Fehrmann, and N. J. Bjerrum, "Complex Formation in Pyrosulfate Melts. 1. Potentiometric, Cryoscopic, and Spectrophotometric Investigations of the Systems Potassium Disulfate-Potassium Sulfate and Otassium Disulfate-Potassium Sulfate-Vanadium Pentoxide in the Temperature Range 410-450. degree. C," *Inorganic Chemistry* 21 (1982): 744.
25. R. W. Berg and N. Thorup, "The Reaction between ZnO and Molten Na₂S₂O₇ or K₂S₂O₇ Forming Na₂Zn (SO₄)₂ or K₂Zn (SO₄)₂, Studied by Raman Spectroscopy and X-ray Diffraction," *Inorganic Chemistry* 44 (2005): 3485.
26. S. Boghosian, R. Fehrmann, N. J. Bjerrum, and G. N. Papatheodorou, "Formation of Crystalline Compounds and Catalyst Deactivation During SO₂ Oxidation in V₂O₅ M₂S₂O₇ (M= Na, K, Cs) Melts," *Journal of Catalysis* (1989): 119.
27. T. Noerbygaard, "The Reaction Between MoO₃ and Molten K₂S₂O₇ Forming K₂MoO₂ (SO₄)₂, Studied by Raman and IR Spectroscopy and X-Ray Crystal Structure Determination," *Procedure* 1998 (1998): 553.
28. V. Wessels and H. A. Höpfe, Unpublished Results.
29. V. Wessels, F. Kraus, L. Bayarjargal, et al., "On The Existence of Highly Condensed Sulfatotungstates and Sulfatomolybdates," *ChemistryEurope* 3 (2025), e202500275.
30. S. Schäffer and R. W. Berg, "Potassium Di-I-Sulfato-1j 2 O: 2j 2 O00-Bis [Cis-Dioxido-Cis-Disulfatotungstate (VI)]," *Acta Crystallographica Section E* 61 (2005): i49–i51.
31. S. J. C. Schäffer and R. W. Berg, "catena-Poly [tetrasodium [[cis-dioxido-trans-bis (sulfato-κO) molybdate (VI)]-μ-sulfato-κ2O: O]]," *Acta Crystallographica Section E* 64 (2008): 173.
32. U. Betke and M. S. Wickleder, "Sulfates of the Refractory Metals: Crystal Structure and Thermal Behavior of Nb₂O₂ (SO₄)₃, MoO₂ (SO₄), WO(SO₄)₂, and Two Modifications of Re₂O₅ (SO₄)₂," *Inorganic Chemistry* 50 (2011): 858.
33. R. Hübenthal, MAPLE. *Program for the Calculation of the Madelung Part of Lattice Energy*, Germany: University of Gießen (1993).
34. R. Hoppe, "Madelung Constants," *Angewandte Chemie International Edition* 5 (1966): 95.
35. R. Hoppe, "The Coordination Number-an "inorganic chameleon,"" *Angewandte Chemie International Edition* 9 (1970): 25.
36. R. Hoppe, "On the Madelung part of Lattice Energy: New Pathways to Use it as a Tool in Solid State Chemistry (Part 1)," *Zeitschrift für Naturforschung* 50 (1995): 555.
37. R. D. Shannon, "Revised Effective Ionic Radii and Systematic Studies of Interatomic Distances in Halides and Chalcogenides," *Acta Crystallographica Section A* 32 (1976): 751.
38. T. Balić Žunić and E. Makovicky, "Determination of the Centroid or "the best centre" of a Coordination Polyhedron," *Acta Crystallographica Section B* 52 (1996): 78.
39. E. Makovicky and T. Balić-Žunić, "New Measure of Distortion for Coordination Polyhedra," *Acta Crystallographica Section B* 54 (1998): 766.
40. A. G. Nord, S. L. Holt, F. Cavalito, K. J. Watson, and M. Sandström, "The Crystal Structure of Cesium Sulfate, beta-Cs₂SO₄," *Acta Chemica Scandinavica* 30a (1976): 198.
41. A. Aird, M. C. Domeneghetti, F. Mazzi, V. Tazzoli, and E. K. H. Salje, "Sheet Superconductivity in WO_{3-x}: Crystal Structure of the Tetragonal Matrix," *Journal of Physics: Condensed Matter* 10 (1998): L569–L574.
42. R. Pascard and C. Pascard-Billy, "Structure Précise de l'anhydride Sulfurique," *Acta Crystallographica* 18 (1965): 830.
43. N. V. Zubkova, I. V. Pekov, D. A. Ksenofontov, V. O. Yapaskurt, D. Y. Pushcharovsky, and E. G. Sidorov, "Arcanite from Fumarole Exhalations of the Tolbachik Volcano (Kamchatka, Russia) and its Crystal Structure," *Doklady Earth Sciences* 479 (2018): 339.
44. J. B. Parise, E. M. McCarron, A. W. Sleight, and E. Prince, "Phase Stability Diagrams of Group 6 Magnéli Oxides and their Implications for Photon-Assisted Applications," *MSF* 27-28 (1988): 85.
45. E. Zintl, A. Harder, and B. Dauth, "Gitterstruktur Der Oxyde, Sulfide, Selenide und Telluride Des Lithiums, Natriums und Kaliums," *Zeitschrift für Elektrochemie Und Angewandte Physikalische Chemie* 40 (1934): 588.
46. F. B. Xiong, D. S. Guo, H. F. Lin, L. J. Wang, H. X. Shen, and W. Z. Zhu, "High-Color-Purity Red-Emitting Phosphors RE₂WO₆: Pr³⁺ (RE= Y, Gd) for Blue LED," *Journal of Alloys and Compounds* 647 (2015): 1121.
47. V. Wessels, S. Kügle, and H. A. Höpfe, "Crystal Structure, Optical Properties and Thermal Properties of M 2 [W 2 O 3 (SO 4) 6](M- Y, Eu, Tb, Lu, Bi)," *Dalton Transactions* 53 (2024): 15703.
48. M. V. Barashkov, A. I. Komyak, and S. N. Shashkov, "Low-Frequency Vibrational Spectra of Crystals of Tutton Salts," *Journal of Applied Spectroscopy* 1 (1999): 100.
49. V. Ramakrishnan, V. U. Nayar, and G. Aruldas, "Vibrational Spectra of LiRbSO₄," *Infrared Physics* 25 (1985): 607.
50. Y. Denisenko, A. S. Aleksandrovsky, V. V. Atuchin, et al., "Exploration of Structural, Thermal and Spectroscopic Properties of Self-Activated Sulfate Eu₂ (SO₄)₃ with Isolated SO₄ Groups," *Journal of Industrial and Engineering Chemistry* 68 (2018): 109.
51. A. Periasamy, S. Muruganand, and M. Palaniswamy, "Vibrational Studies of Na₂SO₄, K₂SO₄, NaHSO₄ and KHSO₄ Crystals," *Rasayan Journal of Chemistry* 4 (2009): 981.
52. R. M. Atkins and K. A. Gingerich, "Matrix Isolation IR and Raman Studies of the Molecules Na₂SO₄ and K₂SO₄," *Chemical Physics Letters* 53 (1978): 347.
53. C. Guery, C. Choquet, F. Dujeancourt, J. M. Tarascon, and J. C. Lassegues, "Infrared and X-Ray Studies of Hydrogen Intercalation in Different Tungsten Trioxides and Tungsten Trioxide Hydrates," *Journal of Solid State Electrochemistry : Current Research and Development in Science and Technology* 1 (1997): 199.
54. M. F. Daniel, B. Desbat, J. C. Lassegues, B. Gerand, and M. Figlarz, "Infrared and Raman Study of WO₃ Tungsten Trioxides and WO₃·xH₂O Tungsten Trioxide Hydrates," *Journal of Solid State Chemistry* 67 (1987): 235.
55. G.-A. Nazri and C. Julien, "Far-Infrared and Raman Studies of Orthorhombic MoO₃ Single Crystal," *Solid State Ionics* 53 (1992): 376.
56. L. Seguin, M. Figlarz, R. Cavagnat, and J. C. Lassegues, "Infrared and Raman Spectra of MoO₃ Molybdenum Trioxides and MoO₃·xH₂O

Molybdenum Trioxide Hydrates,” *Spectrochimica Acta. Part A: Molecular Spectroscopy* 51 (1995): 1323.

57. L. Macalik, P. J. Dereň, J. Hanuza, W. Stręk, A. A. Demidovich, and A. N. Kuzmin, “Effect of Random Distribution and Molecular Interactions on Optical Properties of Er³⁺ dopant in KY (WO₄)₂ and Ho³⁺ in KYb (WO₄)₂,” *Journal of Molecular Structure* 450 (1998): 179.

58. G. Blasse and A. Bril, “On the Eu³⁺ Fluorescence in Mixed Metal Oxides. III. Energy Transfer in Eu³⁺-Activated Tungstates and Molybdates of the Type Ln₂WO₆ and Ln₂MoO₆,” *The Journal of Chemical Physics* 45 (1966): 2350.

59. M. F. A. Hendrickx, V. S. Mironov, L. F. Chibotaru, and A. Ceulemans, “Assignment of the Electronic Spectra of [mo (cn) 8] 4- and [w (cn) 8] 4- by ab Initio Calculations,” *Inorganic Chemistry* 43 (2004): 3142.

60. M. Hämmer, L. Bayarjargal, and H. A. Höpfe, “The First Bismuth Borosulfates Comprising Oxonium and a Tectosilicate-Analogous Anion,” *Angewandte Chemie International Edition* 60 (2021): 1503.

61. M. Hämmer, F. Pielhofer, O. Janka, et al., “Polymorphism and Optical, Magnetic and Thermal Properties of the Either Phyllo- or Inosilicate-Analogous Borosulfate Cu [B₂(SO₄)₄],” *Dalton Transactions* 51 (2022): 3104.

62. E. Turgunbajew and H. A. Höpfe, “The First Antimony Borosulfates Unveil a Modular System MIIIMI [B(SO₄)₂]₄ (MII = Bi³⁺, Sb³⁺, Lu³⁺; MI = H₃O⁺, NO₂⁺, Li⁺, Na⁺, K⁺, Rb⁺, Cs⁺),” *Angewandte Chemie International Edition* (2025): e202424952.

63. G. M. Sheldrick, *SHELXTL*, Karlsruhe, Germany: Bruker AXS, (2003).

64. G. M. Sheldrick, “Crystal Structure Refinement with SHELXL,” *Acta Crystallographica Section C* 71 (2015): 3.

65. V. S. Topas, Karlsruhe, Germany: Bruker AXS (2014).

66. S. K. Kurtz and T. T. Perry, “A Powder Technique for the Evaluation of Nonlinear Optical Materials,” *Journal of Applied Physics* 39 (1968): 3798.

67. L. Bayarjargal, C.-J. Fruhner, N. Schrodt, and B. Winkler, “CaCO₃ Phase Diagram Studied with Raman Spectroscopy at Pressures up to 50 GPa and High Temperatures and DFT Modeling,” *Physics of the Earth and Planetary Interiors* 281 (2018): 31.

68. F. D. Hardcastle and I. E. Wachs, “Molecular Structure of Molybdenum Oxide in Bismuth Molybdates by Raman Spectroscopy,” *The Journal of Physical Chemistry* 95 (1991): 10763.

69. H. Tian, C. A. Roberts, and I. E. Wachs, “Molecular Structural Determination of Molybdena in Different Environments: Aqueous Solutions, Bulk Mixed Oxides, and Supported MoO₃ Catalysts,” *The Journal of Physical Chemistry C* 114 (2010): 14110.

70. N. Buzgar, A. Buzatu, and I. V. Sanislav, “The Raman Study on Certain Sulfates,” *Analele Științifice ale Universității “Alexandru Ioan Cuza” din Iași, Secțiunea I: Matematică* 55 (2009): 5.

71. J. Bode and A. B. van Oosterhout, “Defect Luminescence of Ordered Perovskites A₂BWO₆,” *Journal of Luminescence* 10 (1975): 237.

72. P. Y. Jia, X. M. Liu, G. Z. Li, M. Yu, J. Fang, and J. Lin, “Sol-gel synthesis and characterization of SiO₂@CaWO₄, SiO₂@CaWO₄:Eu³⁺/Tb³⁺ core-shell Structured Spherical Particles,” *Nanotechnol* 17 (2006): 734.

73. M. Colmont, P. Boutinaud, C. Latouche, et al., “Origin of Luminescence in La₂MoO₆ and La₂Mo₂O₉ and their Bi-doped Variants,” *Inorganic Chemistry* 59 (2020): 3215.

74. P. Kaur, R. Kumar, S. Davessar, and A. Khanna, “Structural and Optical Characterization of Er-Doped CaMoO₄ Down-Converting Phosphors,” *Acta Crystallographica Section B* 76 (2020): 926.

Supporting Information

Additional supporting information can be found online in the Supporting Information section. The supporting information contains crystallographic data of all four compounds Cs₆[(WO₂)₂O(SO₄)₄],

K₈[(MoO₂)₂(SO₄)₆], K_{7,9}Sr_{0,1}[(WO₂)₂(SO₄)₆] and Na₄[MoO₂(SO₄)₃], further details on the Rietveld refinement of Cs₆[(WO₂)₂O(SO₄)₄], SHG results of Na₄[MoO₂(SO₄)₃] and the full IR-spectra [15, 21, 29, 37, 40–46, 68–74]. **Supporting Fig. S1:** Experimental powder X-ray diffraction pattern of K₈[(MoO₂)₂(SO₄)₆] compared to the calculated pattern out of single crystal data. **Supporting Fig. S2:** Experimental powder X-ray diffraction pattern of K_{7,9}Sr_{0,1}[(WO₂)₂(SO₄)₆] compared to the calculated pattern out of single-crystal data with a full occupation of the potassium cations. **Supporting Fig. S3:** Experimental powder X-ray diffraction pattern of Na₄[MoO₂(SO₄)₃] compared to the calculated pattern out of single crystal data. **Supporting Fig. S4:** Full FT-IR spectra of all investigated compounds. **Supporting Fig. S5:** Tauc Plots of the isotypic compounds K₈[(MO₂)₂(SO₄)₆] (M = W, Mo) out of the UV-vis data; from the plots it is not unequivocally clear whether a direct or indirect band-gap is present, but in both reasonable cases the band gap is slightly larger for the tungstate compared with the isotypic molybdate which is the relevant conclusion for our discussion in the manuscript. **Supporting Fig. S6:** Thermogram of Cs₆[(WO₂)₂O(SO₄)₄] recorded up to 1500°C in nitrogen atmosphere. **Supporting Fig. S7:** Thermogram of K₈[(MoO₂)₂(SO₄)₆] recorded up to 1050°C in nitrogen atmosphere. **Supporting Fig. S8:** Thermogram of Na₄[MoO₂(SO₄)₃] recorded up to 1050°C in nitrogen atmosphere. **Supporting Fig. S9:** Thermogram of K_{7,9}Sr_{0,1}[(WO₂)₂(SO₄)₆] recorded up to 1500°C in nitrogen atmosphere. **Supporting Fig. S10:** Thermal Ellipsoids of the ions of the two bridging tungstate units at room temperature (left) and 149 K (right). Ellipsoids are shown with a probability of 50%. **Supporting Fig. S11:** Raman spectrum of Na₄[MoO₂(SO₄)₃]. **Supporting Table S1:** Crystal data and details of the structural refinements determined using single-crystal diffraction. The measurement for Cs₆[(WO₂)₂O(SO₄)₄] were performed at T = 149 K. Standard deviations are given in parentheses. **Supporting Table S2:** Atomic coordinates, Wyckoff symbols and isotropic displacement parameters U_{eq} / Å² in Cs₆[(WO₂)₂O(SO₄)₄] at T = 297 K. Standard deviations are given in parentheses. **Supporting Table S3:** Anisotropic displacement parameters U_{ij} / Å² in Cs₆[(WO₂)₂O(SO₄)₄] at T = 297 K. Standard deviations are given in parentheses. **Supporting Table S4:** Atomic coordinates, Wyckoff symbols and isotropic displacement parameters U_{eq} / Å² in Cs₆[(WO₂)₂O(SO₄)₄] at T = 149 K. Standard deviations are given in parentheses. **Supporting Table S5:** Anisotropic displacement parameters U_{ij} / Å² in Cs₆[(WO₂)₂O(SO₄)₄] at T = 149 K. Standard deviations are given in parentheses. **Supporting Table S6:** Atomic coordinates, Wyckoff symbols and isotropic displacement parameters U_{eq} / Å² in K₈[(MoO₂)₂(SO₄)₆]. Standard deviations are given in parentheses. **Supporting Table S7:** Anisotropic displacement parameters U_{ij} / Å² in K₈[(MoO₂)₂(SO₄)₆]. Standard deviations are given in parentheses. **Supporting Table S8:** Atomic coordinates, Wyckoff symbols and isotropic displacement parameters U_{eq} / Å² in K_{7,9}Sr_{0,1}[(WO₂)₂(SO₄)₆]. Standard deviations are given in parentheses. **Supporting Table S9:** Anisotropic displacement parameters U_{ij} / Å² in K_{7,9}Sr_{0,1}[(WO₂)₂(SO₄)₆]. Standard deviations are given in parentheses. **Supporting Table S10:** Atomic coordinates, Wyckoff symbols and isotropic displacement parameters U_{eq} / Å² in Na₄[MoO₂(SO₄)₃]. Standard deviations are given in parentheses. **Supporting Table S11:** Anisotropic displacement parameters U_{ij} / Å² in Na₄[MoO₂(SO₄)₃]. Standard deviations are given in parentheses. **Supporting Table S12:** Selected interatomic distances / Å and angles / ° at T = 149 K in Cs₆[(WO₂)₂O(SO₄)₄]. Standard deviations are given in parentheses. **Supporting Table S13:** Crystal data and structure refinement of Cs₆[(WO₂)₂O(SO₄)₄] determined from powdered data via Rietveld refinement. Respective standard deviations are given in parentheses. **Supporting Table S14:** Ionic radii / pm after Shannon^[1] with respect to their coordination number. **Supporting Table S15:** SHG intensities in quartz, KPD, Al₂O₃ and Na₄[MoO₂(SO₄)₃]. **Supporting Table S12:** Calculated MAPLE values of the binary and tertiary compounds. **Supporting Table S13:** Excitation and emission wavelength of the LMCT in tungstates and molybdates of selected compounds, exhibiting either MO₄ or MO₆ units whether M = W, Mo. **Supporting Table S14:** Assignments of vibrations in the Raman spectrum. **Supporting Table S15:** Summary of energy-dispersive X-ray spectroscopy of Cs₆[(WO₂)₂O(SO₄)₄] of the relevant ions (unfortunately, the main lines of W and Sr occur at the same energy, so always Sr is indicated if W is present in the sample; the further lines of Sr at higher energies imply its absence). **Supporting Table S16:** Summary of

energy-dispersive X-ray spectroscopy of $K_8[(MoO_2)_2(SO_4)_6]$ of the relevant ions. **Supporting Table S17:** Summary of energy-dispersive X-ray spectroscopy of $K_{7.9}Sr_{0.1}[(WO_2)_2(SO_4)_6]$ of the relevant ions (unfortunately, the main lines of W and Sr occur at the same energy, so always Sr is indicated if W is present in the sample; the further lines of Sr at higher energies imply the presence of traces which cannot be quantified safely). **Supporting Table S18:** Summary of energy-dispersive X-ray spectroscopy of $Na_4[MoO_2(SO_4)_3]$ of the relevant ions.